DIGITAL SIMULATION OF CYCLIC CHRONOPOTENTIOMETRY AND CYCLIC RECIPROCAL DERIVATIVE CHRONOPOTENTIOMETRY FOR LINEAR ADSORPTION SYSTEMS

Zygmunt FEKNER

Faculty of Chemistry, Maria Curie-Skłodowska University, M. Curie-Skłodowska Sq. 3, 20-031 Lublin, Poland; e-mail: zygmunt@hermes.umcs.lublin.pl

Received March 12, 2007
Accepted November 19, 2007
Published online March 7, 2008

Digital simulations were applied to generate potential–time response curves for cyclic chronopotentiometry under a constant current in order to gain insight into a reversible charge transfer process at a planar electrode under semi-infinite diffusion conditions. These simulations were carried out for two-species systems in which either both or just one component undergoes adsorption, and this process can be accurately described using the Henry isotherm. From the chronopotentiometric curves obtained, and following their numerical differentiation, the corresponding cyclic reciprocal derivative chronopotentiometric curves were generated and compared with the previously reported analytical solutions. The results obtained according to the proposed simulation scheme were shown to be in perfect agreement with the analytical solutions. It was also demonstrated that digital simulations are a powerful and versatile tool for studying and modeling two-species adsorption systems.
Keywords: Digital simulation; Cyclic chronopotentiometry; Cyclic reciprocal derivative chronopotentiometry; Adsorption; Electrochemistry; Diffusion.

Over the last decades, cyclic chronopotentiometry and cyclic reciprocal derivative chronopotentiometry (CRDCP) have received wide attention[1]. These methods, both in their constant- and programmed-current versions, have been used to study electrode processes, reaction mechanisms, and a plethora of surface phenomena such as adsorption, deposition, passivation, electrochemical corrosion, etc.[2–9]. Recently, it has been suggested that reversible electrode processes can be studied using a new method of current programming, unsymmetrical cyclic reciprocal derivative chronopotentiometry[10]. In this method, the current amplitude for consecutive current steps changes in such a way that the successive transition times are equal to the first transition time. Although CRDCP and classical cyclic voltammetry (CV) curves are superficially similar, the former are by far analytically more useful. It stems from the fact that the peak height on the $dt/dE = f(E)$ curve

Collect. Czech. Chem. Commun. 2008, Vol. 73, No. 2, pp. 201–228

doi:10.1135/cccc20080201

(i.e., on the CRDCP curve) increases as the applied current decreases, thus ensuring that the ohmic drop effects are negligible. Moreover, capacitance effects do not have to be considered in the theoretical description of CRDCP because the appropriate curve parameters are generated from the regions of CRDCP curves for which potential changes, dE/dt, are small. In contrast to CRDCP, one needs to work at high sweep rates to improve the peak high in CV, which leads to an enhancement in the distortion of the I/E curve as a result of the increase of the ohmic drop effects[11,12]. In a series of papers Bi et al.[13,14] presented and tested on real electrochemical systems a simple electronic simulator designed for CRDCP which can be used both in theoretical studies and practical analysis.

The main purpose of the present research was to study, by computer simulation of analytical equations describing both potentiometric curves, $E = f(t)$, and CRDCP curves, dt/d$E = f(E)$, two-species systems in which adsorption of the reactant and/or product occurs. Because peak parameters of the dt/d$E = f(E)$ curves are responsive and sensitive to the occurrence of adsorption in a studied system, they have been successfully applied to investigate such phenomena[3]. They can also provide useful information on the number of species undergoing adsorption and make it possible, by comparison of experimental and theoretical curves, to calculate the relevant adsorption parameters. It should be noted, that in contrast to the analytical equations, presented simulation scheme gives a possibility to obtain concentration profiles of all species at any time of experiment. Besides, the proposed simulation scheme can be easily adapted to modeling cyclic chronopotentiometry and CRDCP with a programmed current of any form.

For many years, digital simulations have been widely used complementarily to both theoretical studies and classical experiments in which diffusion plays an important role. The development of computer simulations over the past decade has been presented in a recent review[15] and a monograph[16].

THEORETICAL

In a series of papers, Molina et al.[2,3] have introduced and tested general analytical equations describing changes of the surface concentration of the oxidized (A) and reduced (B) species at a planar electrode during consecutive cycles of a chronopotentiometric experiment. These equations have been derived in accordance with the superposition principle while, at the same time, taking into consideration the following assumptions[2]:

a) Charge transfer reaction described by Eq. (*1*) is reversible.

$$\mathrm{A} + n\mathrm{e} \Leftrightarrow \mathrm{B} \qquad (1)$$

b) Adsorption of the species can be described using the Henry isotherm, $\Gamma_i = K_i c_i(0,t)$, with adsorption constants, K_i, being independent of the electrode potential within the range in which the experiment is conducted.

c) Both the surface excess, Γ_i, of the reactant (A) and product (B) as well as their volume concentrations are continuously in equilibrium, i.e., the adsorption process is so fast that it is limited only by the diffusion-controlled mass transport, and not by the rate of adsorption.

It was also arbitrarily chosen that the odd current steps (j = 1, 3, 5...) were cathodic. Conversely, the even current steps (j = 2, 4, 6...) were chosen to be anodic.

Equations (*1*) and (*2*) presented by Molina et al.[3], describing the change in the surface concentration of species A and B, $c^j_{i,0}(t)$, during the j-th current step while in the following (j + 1)-th step the electrode is polarized with the current of the same value but of the opposite sign, i.e., $I_j = (-1)^{j+1} I_0$ (the symmetrical programmed current according to the classification introduced elsewhere[10]), can be transformed as follows:

$$c^j_{\mathrm{A},0}(t)/c^0_{\mathrm{A}} = 1 - Z_{\mathrm{A}}\left(t^{1/2}_{1,j} H\left(\chi^{\mathrm{A}}_{1,j}\right) + 2\sum_{n=2}^{j}(-1)^{j+1} t^{1/2}_{n,j} H\left(\chi^{\mathrm{A}}_{n,j}\right)\right) \qquad (2a)$$

$$c^j_{\mathrm{B},0}(t)/c^0_{\mathrm{B}} = \mu + Z_{\mathrm{B}}\left(t^{1/2}_{1,j} H\left(\chi^{\mathrm{B}}_{1,j}\right) + 2\sum_{n=2}^{j}(-1)^{j+1} t^{1/2}_{n,j} H\left(\chi^{\mathrm{B}}_{n,j}\right)\right) \qquad (2b)$$

where

$$Z_i = 2I/nFAc^0_{\mathrm{A}}(D_i\pi)^{1/2} \quad i = \mathrm{A}, \mathrm{B}\,. \qquad (3)$$

Obviously, if the diffusion coefficients, D_i, for the two species are equal, then $Z_{\mathrm{A}} = Z_{\mathrm{B}}$.

$$\chi^i_{n,j} = (D_i t_{n,j})^{1/2} K_i^{-1} \quad i = \mathrm{A}, \mathrm{B} \qquad (4)$$

$$t_{n,j} = \sum_{k=n}^{j-1} \tau_k + t_j \quad n < j \tag{5}$$

$$t_{j,j} = t_j \tag{6}$$

$$\mu = c_B^0 / c_A^0 \tag{7}$$

where τ_k is the cathodic (k odd) or anodic (k even) transition time corresponding to the k-th current step applied; t_j is the time that passed since the beginning of the j-th current step; c_i^0 is the starting concentration (i.e., at $t = 0$) of the i-th species in solution; A is the electrode area; F, n, and I retain their customary meanings.

The total time, t, of the experiment is given by

$$t = \sum_{k=1}^{j-1} \tau_k + t_j \,. \tag{8}$$

The $H(x)$ function present in Eqs (*2a*) and (*2b*) is described by the following equations[2] (after the upper limit of the product in the numerator of the first formula was adjusted as presented in Eq. (*9*)):

$$H(x) = \begin{cases} \displaystyle\sum_{j=1}^{\infty} \frac{(-1)^{j+1} \prod_{i=1}^{j} p_i x^j}{(j+1)!} & x \le 5 \\ \displaystyle 1 - \frac{\sqrt{\pi}}{2} x^{-1} + \frac{1}{2} x^{-2} - \frac{1}{4} x^{-4} + \frac{3}{8} x^{-6} - \frac{15}{16} x^{-8} + \frac{105}{32} x^{-10} - \ldots & x > 5 \end{cases} \tag{9}$$

where

$$p_i = \frac{2\Gamma(1 + i/2)}{\Gamma((1+i)/2)} \,. \tag{10}$$

In Eq. (*10*), Γ is the gamma function.

The $H(x)$ function has the following limiting values[17]:

$$\lim H(x) = \begin{cases} 1 & \text{when } x \to \infty \\ 0 & \text{when } x \to 0 \end{cases} . \tag{11}$$

The values of the $H(x)$ function can also be calculated from the following formula[3]:

$$H(x) = 1 - (\pi^{1/2}/2x)(1 - \exp(x^2)\,\mathrm{erfc}(x)) \qquad (12)$$

where $\mathrm{erfc}(x) = 1 - \mathrm{erf}(x)$ is the complementary error function and $\mathrm{erf}(x)$ is the error function.

The dependence of the electrode potential, E, on the duration of the j-th current step (i.e., the chronopotentiogram) can be obtained by merging Eqs (*2a*) and (*2b*) with the Nernst equation:

$$E(t) = E^{\circ} + (RT/nF)\ln\left(c^{j}_{\mathrm{A},0}(t)\big/c^{j}_{\mathrm{B},0}(t)\right) \qquad (13)$$

where E° is the standard potential, R is the gas constant, and T is the absolute temperature.

It should be noted that the equations introduced by Molina et al.[2,3] make it possible to calculate the concentration of species A and B on the electrode surface. However, they are not suitable for the determination of the concentration profiles for species A and B in the bulk solution for any moment during the experiment.

Simulation Method

The simulations were carried out using the point method, which is based on finite-difference approximations of derivatives in Fick's second diffusion equation[16] with equal intervals of both (dimensionless) time $\overline{T}$, $(0, \delta\overline{T}, 2\delta\overline{T}...)$ and space $(0, h, 2h...)$.

Because in digital simulations it is convenient to normalize all variables (in order to obtain more general and useful solutions), in the present research this normalization was performed in accordance with the method described, among others, by Britz[16] and Bieniasz[18], namely:

$$C_i = c_i/c^{0}_{\mathrm{A}} \qquad (14)$$

$$\overline{D}_i = D_i/D_{\mathrm{A}} \qquad (15)$$

$$\overline{K}_i = K_i / K_A \tag{16}$$

$$X = x / (D_A \tau)^{1/2} \tag{17}$$

$$\bar{I} = I / I_{norm} = I\tau^{1/2} / nFAc_A^0 D_A^{1/2} \tag{18}$$

$$\overline{T} = t / \tau \tag{19}$$

$$p = (E - E^o)(nF/RT) \tag{20}$$

where C_i, $\overline{D}_i$, $\overline{K}_i$ are the dimensionless concentration, diffusion coefficient, and adsorption constant of *i*-th species, respectively; *x* and *X* are the dimensioned and dimensionless distances from the electrode, respectively, and $\bar{I}$, *p* are the dimensionless current and potential, respectively.

In Eqs (*17*), (*18*), and (*19*), τ is some fixed experimental (observation) time (i.e., the reference time scale). For simulations of chronopotentiometry, it is commonly recommended to take τ equal to the transition time obtained from the Sand equation (i.e., for an uncomplicated, fully reversible charge transfer reaction under pure diffusion conditions)[16]. Needless to say, the above described strategy cannot be effectively applied to systems in which a species undergoes adsorption. For such systems, even the first dimensionless transition time, $\overline{\tau}_1$, would be much higher than the unity (see, for example, Tables 1–3 in Molina et al.[2] and Tables 3–5 in Molina et al.[3]).

The total (dimensionless) time of the simulation experiment, $\overline{T}_{total}$, is equal to:

$$\overline{T}_{total} = \sum_{i=1}^{j} \overline{\tau}_i = t / \tau \tag{21}$$

where $\overline{\tau}_i = \tau_i / \tau$ is the *i*-th dimensionless transition time.

The size of the simulated system cannot be smaller than the thickness of the diffusion layer (multiplied by a small factor, most frequently 6), i.e., $6(\overline{D}_{max}\, \overline{T}_{total})^{1/2}$ (where $\overline{D}_{max}$ is the maximum dimensionless diffusion coefficient of all the involved species). Therefore, for large values of $\overline{T}_{total}$, the simulated system must also be large. This, in turn, renders the correspond-

ing simulation excessively time-consuming. This is especially apparent during digital simulations of multicyclic processes that are the subject of the present studies. To circumvent this serious practical obstacle, we assumed that the observation time, τ, was equal to the first transition time for the adsorption system studied, i.e., $\tau = \tau_1^{ads}$. Its relation to the adsorption constant is given as follows[2]:

$$(\tau_1^{ads})^{1/2} = \frac{nFAc_A^0(D_A\pi)^{1/2}}{2IH\left((D_A\tau_1^{ads})^{1/2}K_A^{-1}\right)} = \frac{Z_A^{-1}}{H\left((D_A\tau_1^{ads})^{1/2}K_A^{-1}\right)} . \qquad (22)$$

Taking into account Eq. (*11*), it is apparent that, for $K_A \to 0$, Eq. (*22*) converts to the Sand equation. It also needs to be pointed out that, when the observation time, τ, is selected according to the method described above, i.e., $\tau = \tau_1^{ads}$, the dimensionless current, $\bar{I}$, can be given as

$$\bar{I} = \frac{\pi^{1/2}}{2H\left((D_A\tau_1^{ads})^{1/2}K_A^{-1}\right)} \qquad (23)$$

which is a direct consequence of Eqs (*18*) and (*22*).

The dimensionless current, $\bar{I}$, defined in this manner, reduces (but only when $K_A \to 0$, i.e., the charge transfer occurs under pure diffusion conditions), to the familiar value of $\sqrt{\pi}/2$ (i.e., to the dimensionless current under pure diffusion conditions).

Thanks to such a choice of the reference time scale, $\tau = \tau_1^{ads}$, the first dimensionless transition time, $\bar{\tau}_1$, for any adsorption system is reached (or, at least, should be reached) during the simulation after $\bar{T} = 1$. This is analogous to simulations of chronopotentiometry under pure diffusion conditions for which the observation time, τ, is taken as the transition time obtained from the Sand equation. The only inconvenience, albeit small, associated with the method of selecting the observation time that was used in our studies is related to the fact that τ_1^{ads} is present on both sides of Eq. (*22*). As a consequence, its value has to be determined numerically, for example, by the bisection method. It is especially important for those who would like to correlate the dimensionless results of their simulations with the parameters measured for real systems.

In the present simulation scheme, partial differential equations (PDEs), as well as initial and boundary conditions, comprise the basis of any simulation. PDEs, for which the solutions are given by Eqs (*2a*) and (*2b*), when expressed with dimensionless variables, are as follows:

a) Governing PDEs (second Fick's law):

$$\frac{\partial C_{\mathrm{A}}}{\partial \overline{T}} = \frac{\partial^2 C_{\mathrm{A}}}{\partial^2 X}\,, \quad \frac{\partial C_{\mathrm{B}}}{\partial \overline{T}} = d\,\frac{\partial^2 C_{\mathrm{B}}}{\partial^2 X} \tag{24}$$

where $d = D_{\mathrm{B}}/D_{\mathrm{A}}$.

b) The initial and boundary conditions[2]:

$$\left.\begin{array}{l} \overline{T} = 0,\ X \geq 0 \\ \overline{T} \geq 0,\ X \to \infty \end{array}\right\} \quad C_{\mathrm{A}} = 1, \quad C_{\mathrm{B}} = \mu \tag{25}$$

$$T > 0,\ X = 0 \quad \frac{\partial C_{\mathrm{A},0}}{\partial \mathrm{X}} = \bar{I} + K'_{\mathrm{A}}\left(\frac{\partial C_{\mathrm{A},0}}{\partial \overline{T}}\right), \quad d\,\frac{\partial C_{\mathrm{B},0}}{\partial \mathrm{X}} = -\bar{I} + d^{1/2} K'_{\mathrm{B}}\left(\frac{\partial C_{\mathrm{B},0}}{\partial \overline{T}}\right) \tag{26}$$

where $K'_{\mathrm{A}}, K'_{\mathrm{B}}$ are the coefficients resulting from normalizations

$$K'_{\mathrm{A}} = K_{\mathrm{A}}\left(D_{\mathrm{A}}\tau_1^{\mathrm{ads}}\right)^{-1/2} \tag{27}$$

$$K'_{\mathrm{B}} = K_{\mathrm{B}}\left(D_{\mathrm{B}}\tau_1^{\mathrm{ads}}\right)^{-1/2} \tag{28}$$

and are related as follows:

$$K'_{\mathrm{B}} = d^{-1/2}\, k K'_{\mathrm{A}} \tag{29}$$

where

$$k = K_{\mathrm{B}}/K_{\mathrm{A}}\ . \tag{30}$$

As it can be noted, certain derivative boundary conditions, Eq. (*26*), are present in our model. The commonly known problem, associated with the classical Crank–Nicolson (CN) scheme utilized in our work as well, is related to difficulties arising when the boundary conditions are given in such a form[16]. To overcome this obstacle, we used a modified algorithm of the CN scheme in which implicit forms of the boundary conditions, Eq. (*26*), are included. This particular scheme involves incorporating concentrations on the electrode surface at the time $\overline{T} + \delta\overline{T}$ (which are, at that particular

moment, yet unknown) into the implicit equations generated when using the CN method[16,19,20].

Discretization of Eqs (*24*) was carried out in the usual manner as detailed elsewhere[16]:

$$C'_{i,j} - C_{i,j} = \frac{\lambda_i}{2}(C_{i,j-1} - 2C_{i,j} + C_{i,j+1} + C'_{i,j-1} - 2C'_{i,j} + C'_{i,j+1}) \qquad (31)$$
$$i = \mathrm{A, B}; \quad j = 1, m$$

where $\lambda_i = \overline{D}_i \delta T / h^2$ ($h \equiv \delta X$ is the space interval along x); $C_{i,j}$ are the known concentrations at the time $\overline{T}$, whereas $C'_{i,j}$ are the new, yet-to-be-established concentrations of the i-th species in the j-th point of the space grid at the time $\overline{T} + \delta\overline{T}$, and m is the number of points in the space grid.

In order to discretize the right-hand sides of Eqs (*26*), the following two-point formula was used:

$$\frac{\partial C_{i,0}}{\partial \overline{T}} \approx \frac{C'_{i,0} - C_{i,0}}{\delta \overline{T}} . \qquad (32)$$

The concentration gradient of the i-th species at the electrode at time $\overline{T} + \delta\overline{T}$, $G'_i = (\partial C'_{i,0}/\partial X)$, was discretized using the following five-point forward approximation:

$$G'_i \approx \frac{1}{A_5 h}\sum_{n=0}^{4} B_n C'_{i,n} = \frac{1}{12h}(-25C'_{i,0} + 48C'_{i,1} - 36C'_{i,2} + 16C'_{i,3} - 3C'_{i,4}) \quad i = \mathrm{A,B}. \qquad (33)$$

By combining Eqs (*26*), (*32*), and (*33*), the following equations were obtained:

$$\beta'_{i,0} C'_{i,0} + \sum_{n=1}^{4} B_n C'_{i,n} = \gamma_i \quad i = \mathrm{A, B} \qquad (34)$$

where

$$\beta'_{\mathrm{A},0} = \left(-25 - \frac{12K'_{\mathrm{A}} h}{\delta \overline{T}}\right) \qquad (35a)$$

$$\beta'_{\mathrm{B},0} = \left(-25 - \frac{12K'_{\mathrm{B}} h d^{-1/2}}{\delta \overline{T}}\right) \qquad (35b)$$

$$\gamma_{\mathrm{A}} = 12h\left(\bar{I} - \frac{K'_{\mathrm{A}} C_{\mathrm{A},0}}{\delta\overline{T}}\right) \tag{36a}$$

$$\gamma_{\mathrm{B}} = -12h\left(\bar{I}d^{-1} + \frac{K'_{\mathrm{B}} C_{\mathrm{B},0} d^{-1/2}}{\delta\overline{T}}\right). \tag{36b}$$

Equations (*34*), in combination with the first four equations of the set (*31*), made it possible to determine the implicit new concentrations of species A and B at the electrode, $C'_{\mathrm{A},0}$ and $C'_{\mathrm{B},0}$, respectively. With these concentrations established, solving the set of Eqs (*31*) leads to the new concentration profiles (at the time $\overline{T} + \delta\overline{T}$) for species A and B. As it can be seen, the computer simulations provide the entire concentration profile for the *i*-th species at any given time. This cannot be accomplished when the analytical equations proposed by Molina et al.[2,3] are used.

For the simulated systems, at the beginning of the simulation ($\overline{T} = 0$), the initial concentrations of species A and B were set as follows:

$$C_{\mathrm{A}}(X, \overline{T} = 0) = 1, \quad C_{\mathrm{B}}(X, \overline{T} = 0) = \mu \quad \text{for all } X\,. \tag{37}$$

Next, for any subsequent time step, new concentration profiles for species A and B were calculated. With the new concentration profiles in hand, the dimensionless potential, *p*, was determined in accordance with Eq. (*38*):

$$p(\overline{T}) = \ln\left[C_{\mathrm{A},0}(\overline{T}) / C_{\mathrm{B},0}(\overline{T})\right]. \tag{38}$$

The above equation was obtained by applying the normalization rules expressed by Eqs (*14*) and (*20*) to the Nernst equation, Eq. (*13*). The simulation of any given current step was carried out until $C'_{\mathrm{A},0}$ (for odd values of *j*) or $C'_{\mathrm{B},0}$ (for even values of *j*) became non-positive. Because it was very unlikely that a simulation of any given current step would terminate when either $C'_{\mathrm{A},0}$ or $C'_{\mathrm{B},0}$ was exactly zero (obviously, most of the time it was negative), and in order to avoid a situation where at the beginning of the next current step either $C'_{\mathrm{A},0}$ or $C'_{\mathrm{B},0}$ was negative, the entire concentration profiles were interpolated in such a way as to ensure that the next (*j* + 1)-th current step would commence with $C'_{\mathrm{A},0} = 0$ (for odd values of *j*) or $C'_{\mathrm{B},0} = 0$

(for even values of j). The dimensionless transition time, $\overline{\tau}_j$, determined during the j-th simulation, was adjusted in an analogous manner.

In the present studies, all the simulations were carried out using the parameters $d = 1$ (i.e., for equal diffusion coefficients for species A and B), $\lambda_A = \lambda_B = 5.0$, and $\delta\overline{T} = 1.0 \times 10^{-4}$.

Validation

In order to compare the results of our simulations with those obtained by Molina et al.[3] based on Eqs (*2a*) and (*2b*), it was necessary to present these equations in the dimensionless form. The normalization was carried out using the transformations depicted in Eqs (*14*)–(*16*), (*18*), and (*19*). After Eqs (*22*) and (*23*) were also taken into consideration, the following equations were obtained:

$$C^j_{A,0}(\overline{T}) = 1 - \left[H(1/K'_A)\right]^{-1}\left[\overline{T}^{1/2}_{1,j} H\left(\overline{T}^{1/2}_{1,j}/K'_A\right) + 2\sum_{n=2}^{j}(-1)^{j+1}\overline{T}^{1/2}_{n,j} H\left(\overline{T}^{1/2}_{n,j}/K'_A\right)\right]$$

for $K'_A > 0$ and $K'_B \geq 0$ (*39a*)

$$C^j_{B,0}(\overline{T}) = \mu + d^{-1/2}\left[H(1/K'_A)\right]^{-1}\left[\overline{T}^{1/2}_{1,j} H\left(\overline{T}^{1/2}_{1,j}/K'_B\right) + 2\sum_{n=2}^{j}(-1)^{j+1}\overline{T}^{1/2}_{n,j} H\left(\overline{T}^{1/2}_{n,j}/K'_B\right)\right]$$

for $K'_A > 0$ and $K'_B > 0$ (*39b*)

where $\overline{T}_{n,j} = t_{n,j}/\tau_1^{ads}$, $\overline{T} = \overline{T}_{1,j}$. For $t_{n,j}$, see Eq. (*5*).

Because Eqs (*39a*) and (*39b*) are valid only for the positive values of K'_A and K'_B (strictly speaking, Eq. (*39a*) is also valid for $K'_B = 0$), it was necessary to use the limiting values of the $H(x)$ function set in Eq. (*11*) in order to arrive at equations describing the surface concentrations of the species that does not undergo adsorption ($K'_i = 0$, i = A, B). Taking the above into account, the following equations were obtained:

$$C^j_{A,0}(\overline{T}) = 1 - \left(\overline{T}^{1/2}_{1,j} + 2\sum_{n=2}^{j}(-1)^{j+1}\overline{T}^{1/2}_{n,j}\right)$$

for $K'_A = 0$ and $K'_B \geq 0$ (*40*)

$$C^{j}_{\mathrm{B},0}(\overline{T}) = \mu + d^{-1/2}\left[H(1/K'_{\mathrm{A}})\right]^{-1}\left(\overline{T}^{1/2}_{1,j} + 2\sum_{n=2}^{j}(-1)^{j+1}\,\overline{T}^{1/2}_{n,j}\right)$$

$$\text{for } K'_{\mathrm{B}} = 0 \text{ and } K'_{\mathrm{A}} > 0 \qquad (41a)$$

$$C^{j}_{\mathrm{B},0}(\overline{T}) = \mu + d^{-1/2}\left(\overline{T}^{1/2}_{1,j} + 2\sum_{n=2}^{j}(-1)^{j+1}\,\overline{T}^{1/2}_{n,j}\right)$$

$$\text{for } K'_{\mathrm{B}} = K'_{\mathrm{A}} = 0\,. \qquad (41b)$$

RESULTS AND DISCUSSION

For the sake of simplicity, we introduced a classification of the adsorption systems studied. If in a given system, both species A and B undergo adsorption, such a system is assigned to be of the AB type. Analogously, when either species A (but not species B) or species B (but not species A) undergoes adsorption, such a system is assigned to be of the A or B type, respectively.

In order to check the accuracy of our digital simulation scheme, a wide range of simulation calculations were carried out. The simulation parameters were selected in such a way that would enable us to arrive at the results, including consecutive transition times, full chronopotentiograms, CRDCP curves and their parameters, analogous to those presented by Molina et al.[3] To demonstrate the effectiveness of our computer simulations, the calculations were performed for the first 25 full cycles (i.e., 50 consecutive current steps) for adsorption systems of all the three types described above. Although Molina et al.[3] presented their results for the first cycle only (i.e., for a sequence of one cathodic and one anodic step), we carried out our own calculations for 25 cycles based on the analytical equations (*38*), (*39a*), and (*39b*).

The AB-Type Adsorption Systems ($K'_{\mathrm{A}} \neq 0$ and $K'_{\mathrm{B}} \neq 0$)

In Table I, the analytical calculation (dimensioned) parameters and the corresponding simulation parameters for the AB-type adsorption systems studied are summarized. In addition, the parameters for systems in which neither species A nor B undergoes adsorption, i.e., the systems characterized by the reversible charge transfer under semi-infinite diffusion conditions, are also presented. Throughout the manuscript, we attached the

"diff" tag to such systems. The parameter $\Omega = \Gamma_{0,B}/\Gamma_{0,A}$ used by Molina et al.[3] and the parameter μ are related in the following manner:

$$\Omega = k\mu \tag{42}$$

where $\Gamma_{0,A}$ and $\Gamma_{0,B}$ are the surface excess of species A and B, respectively, at the beginning of the experiment.

It can also be noted that Eq. (*42*) is true only when $k \neq 0$.

The analytical calculations were based on Eqs (*39a*) and (*39b*), with the time increment $\delta\bar{T} = 1.0 \times 10^{-4}$. As it was the case for our digital simulations, a present current step was terminated when either $C'_{A,0}$ (for odd values of *j*) or $C'_{B,0}$ (for even values of *j*) became non-positive. Similarly, the calculated transition time was subsequently adjusted in such a fashion as to ensure that the corresponding concentration of an appropriate species was exactly zero at the end of a given step. Needless to say, the concentration of the other species was also adjusted by assuming that changes in the concentration of the two species were linear over the time period equal to $\delta\bar{T}$. The

TABLE I
Analytical-calculation parameters and corresponding simulation parameters for AB-type adsorption systems

$Z_A = Z_B = 3\,s^{-1/2}$ $D_A = D_B$ $\frac{\sqrt{D_A}}{K_A} = \frac{\sqrt{D_B}}{K_B}$, $s^{-1/2}$	$\Omega = \mu = 0$ and $\Omega = \mu = 0.5$ $d = 1 \quad k = 1$ Simulation parameters		
	$\sqrt{\tau_1^{ads}}$ Eq. (*22*)	$K'_A = K'_B$ Eq. (*27*) and (*28*)	$\bar{I}$ Eq. (*23*)
Diff	0.333333	0.000000	0.886227
1	0.779855	1.282290	2.073385
0.1	2.088585	4.787930	5.552882
0.05	2.889617	6.921333	7.682568
0.01	6.276829	15.931612	16.68808

calculations for the systems in which neither species undergoes adsorption (i.e., the "diff"-tagged systems in Table I) were based on Eqs (*40*) and (*41b*).

In Fig. 1, the calculated relative transition times, $\bar{\tau}_{ref}$, obtained from the simulations and analytical equations (*39a*) and (*39b*), for the AB-type adsorption systems ($\mu = 0$) are compared. Figure 1a-2 shows the dependence of relative transition times, $\bar{\tau}_{ref}$, on the current-step number, *j*, for the AB-type adsorption systems studied ($\mu = 0$), whereas Fig. 1a-1 shows the changes of the err function (see Eq. (*44*)) with the current-step number, *j*. The relative transition time, $\bar{\tau}_{ref}$, and the err function are defined as follows:

$$\bar{\tau}_{ref} = \begin{cases} \bar{\tau}_j / \bar{\tau}_1 & \text{for odd values of } j \\ \bar{\tau}_j / \bar{\tau}_2 & \text{for even values of } j \end{cases} \qquad (43)$$

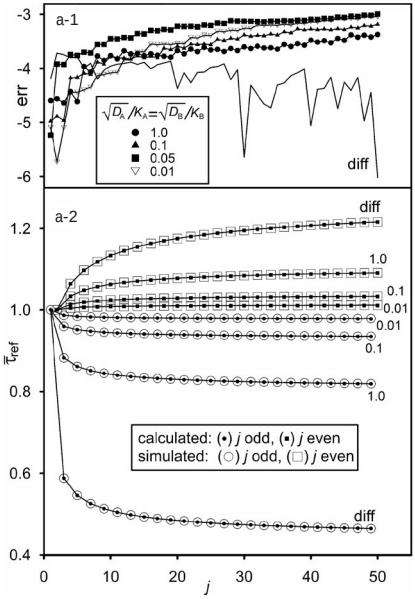

FIG. 1

Cyclic chronopotentiometry. Comparison of changes of relative transition times, $\bar{\tau}_{ref}$, according to Eq. (*43*) (Fig. 1a-2) obtained from analytical equations (*39a*) and (*39b*), (● for odd values of *j*, ■ for even values of *j*) and simulation results (○ for odd values of *j*, □ for even values of *j*) for AB-type adsorption systems ($\mu = 0$). Dependence of the err function values according to Eq. (*44*) from the current-step number, *j* (Fig. 1a-1). Values of $\sqrt{D_A} / K_A = \sqrt{D_B} / K_B$ in $s^{-1/2}$ are included on the graphs. Diff curves correspond to a pure diffusion process. Analytical-calculation and simulation parameters for systems depicted here are summarized in Table I. For clarity, only selected $\bar{\tau}_{ref} = f(j)$ curves are presented

$$\mathrm{err}\,(j) = \log\left(\left|\bar{\tau}_j^{\mathrm{calc}} - \bar{\tau}_j^{\mathrm{sim}}\right| \Big/ \bar{\tau}_j^{\mathrm{calc}}\right) \qquad (44)$$

where $\bar{\tau}_j^{\mathrm{calc}}$ and $\bar{\tau}_j^{\mathrm{sim}}$ are the j-th dimensionless transition times obtained from the analytical equations (calc) and simulations (sim), respectively.

In Fig. 2 are presented the dimensionless chronopotentiometric and dimensionless CRDCP curves (the first cycle, i.e., the first cathodic and an-

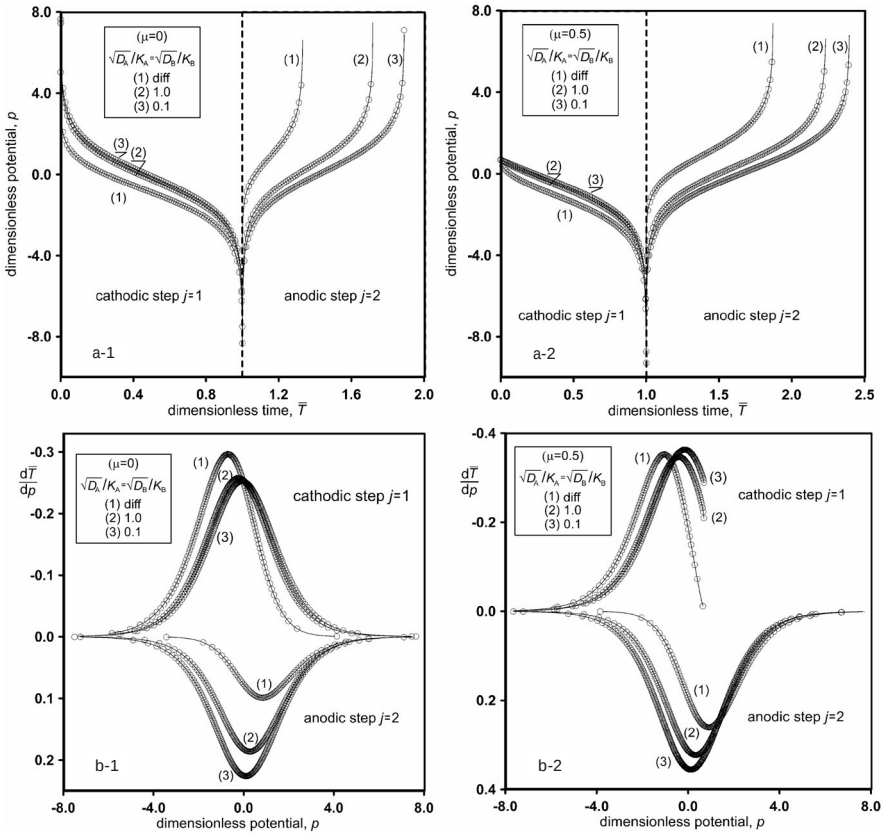

FIG. 2

First cycle of cyclic chronopotentiometry and CRDCP. Comparison of potential–time response curves (Fig. 2a-1 for μ = 0, Fig. 2a-2 for μ = 0.5) and $\mathrm{d}\bar{T}/\mathrm{d}p$ vs dimensionless potential, p, curves (Fig. 2b-1 for μ = 0, Fig. 2b-2 for μ = 0.5) for AB-type adsorption systems obtained from analytical equations (solid lines) and simulations (○). $\sqrt{D_A}\,/\,K_A = \sqrt{D_B}\,/\,K_B$ in $s^{-1/2}$ are: (1) diff, (2) 1.0, (3) 0.1. For clarity, only selected curves and reduced number of simulation points are presented

odic current steps) for the AB-type adsorption systems obtained from the simulations (○) and analytical equations (solid lines). Figures 2a-1 and 2a-2 compare dimensionless chronopotentiometric curves (Fig. 2a-1 for $\mu = 0$ and Fig. 2a-2 for $\mu = 0.5$) obtained from the simulations (○) and analytical equations (solid lines) (*38*), (*39a*), and (*39b*). Figures 2b-1 and 2b-2 compare dimensionless CRDCP curves (Fig. 2b-1 for $\mu = 0$ and Fig. 2b-2 for $\mu = 0.5$). The presented curves, generated by numerical differentiation of dimensionless chronopotentiometric curves resulting from our simulations, were juxtaposed with those obtained from the analytical equations (*38*), (*39a*), and (*39b*). The five-point first-derivative approximation (fourth order $O(h^4)$, central-difference approximation, see Table A.1, Appendix 1 in ref.[16] for coefficients) was applied.

In Fig. 3, the dimensionless concentration profiles of A (solid lines) and B species (dashed lines) reached during the first (cathodic) current step after $\overline{T} = 0.1, 0.3, 0.5, 1.0$ for a selected AB-type system are presented (Fig. 3a-1 for $\mu = 0$ and Fig. 3a-2 for $\mu = 0.5$).

Table II shows the comparison between the parameters for the dimensionless chronopotentiometric and CRDCP curves obtained from the analytical equations and simulations for the AB-type adsorption systems studied. In Table II, $R_y^{j-1,j}$ and $\Delta p^{j,j-1}$ are the ratio of the cathodic and anodic peak

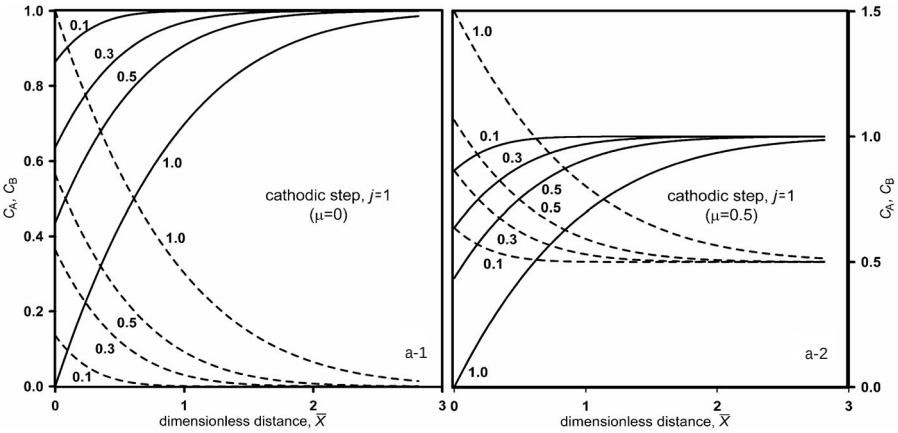

FIG. 3

Dimensionless concentration profiles for A (solid lines) and B species (dashed lines) reached during first current step for selected AB-type adsorption system ($\sqrt{D_A} / K_A = \sqrt{D_B} / K_B = 1.0 s^{-1/2}$, Fig. 3a-1 for $\mu = 0$, Fig. 3a-2 for $\mu = 0.5$) after $\overline{T} = 0.1, 0.3, 0.5, 1.0$

heights and the distance between the cathodic and anodic dimensionless peak potentials, respectively. These two parameters are defined as follows[3]:

$$R_y^{j-1,j} = \left| y_c^{j-1,\max} \Big/ y_a^{j,\min} \right| \quad j = 2, 4, 6\ldots \tag{45}$$

$$\Delta p^{j,j-1} = p_a^{j,\min} - p_c^{j-1,\max} \quad j = 2, 4, 6\ldots \tag{46}$$

where $y_c^{j-1,\max}$ and $y_a^{j,\min}$ are the cathodic and anodic dimensionless peak heights, respectively, whereas $p_c^{j-1,\max}$ and $p_a^{j,\min}$ are the cathodic and anodic dimensionless peak potentials, respectively.

TABLE II
Comparison of parameters of dimensionless chronopotentiometric and CRDCP curves for AB-type adsorption systems obtained from digital simulations and analytical equations (in parentheses) for the first cycle

$\frac{\sqrt{D_A}}{K_A} = \frac{\sqrt{D_B}}{K_B}$, $s^{-1/2}$	$\Omega = \mu = 0$				$\Omega = \mu = 0.5$			
	$\bar{\tau}_1$	$\bar{\tau}_2$	$R_y^{1,2}$	$\Delta p^{2,1}$	$\bar{\tau}_1$	$\bar{\tau}_2$	$R_y^{1,2}$	$\Delta p^{2,1}$
Diff	1.0001 (1.0000)	0.3334 (0.3333)	3.0007 (2.9976)	1.5423 (1.5316)	1.0001 (1.0000)	0.8729 (0.8728)	1.3516 (1.3513)	1.9473 (1.9406)
1.00	1.0000 (1.0000)	0.7188 (0.7188)	1.3857 (1.3835)	0.5172 (0.5113)	1.0000 (1.0000)	1.2351 (1.2351)	1.0747 (1.0751)	0.7465 (0.7408)
0.10	1.0000 (1.0000)	0.8912 (0.8912)	1.1177 (1.1166)	0.1774 (0.1786)	1.0000 (1.0000)	1.3977 (1.3977)	1.0218 (1.0218)	0.2674 (0.2693)
0.05	1.0000 (1.0000)	0.9207 (0.9207)	1.0817 (1.0818)	0.1275 (0.1280)	1.0000 (1.0000)	1.4255 (1.4255)	1.0155 (1.0151)	0.1961 (0.1945)
0.01	0.9999 (1.0000)	0.9630 (0.9631)	1.0366 (1.0362)	0.02966 (0.02968)	0.9999 (1.0000)	1.4652 (1.4653)	1.0065 (1.0065)	0.0893 (0.0896)

The A-Type Adsorption Systems ($K'_A \neq 0$, $K'_B = 0$)

As it was pointed out earlier, Eqs (*39a*) and (*39b*) can be applied only when $K'_i > 0$. This precondition certainly limits the applicability of these equations. It has its origin in the way the equations were originally solved, i.e., while introducing the dimensionless variable χ_i, it was assumed that the adsorption constants must be positive (see Eq. (A.1) in Appendix A in Molina et al.[2]). For example, in order to calculate $C_{B,0}^j(\bar{T})$ there are three equations,

Eqs (*39b*), (*41a*), and (*41b*), that could, in principle, be used. However, none of them can be used to study the B-type adsorption systems as K'_A is equal exactly zero, and it cannot be artificially set at a positive, no matter how small, value. In particular, Eqs (*39b*) and (*41a*) are not applicable here because they can only be used for positive values of K'_A (i.e., for the AB-type adsorption systems), whereas Eq. (*41b*) can only be used when $K'_B = 0$ (by definition, for the B-type adsorption systems, K'_B is positive). Another problem encountered when either the A- or B-type adsorption systems for which $\mu > 0$ are studied is related to the fact that it is not possible to use Eq. (*42*) that allows to connect the parameter μ with the parameter Ω that was used elsewhere[3]. Equation (*42*) can only be used when the parameter *k*, defined according to Eq. (*30*), is positive. In other words, both K'_A and K'_B need to be positive, and this precondition is never met by either the A- or B-type adsorption systems. To be precise, Eqs (*39a*) and (*41a*) could be used for the A-type adsorption systems but only when $\mu = 0$. In practice, however, in order to carry out the calculations for the A-type (as well as B-type) adsorption systems for any value of μ, it is necessary to assign a very small positive value to the appropriate adsorption coefficient, $K'_i = \varepsilon$. Owing to the limiting values of the $H(x)$ function described by Eq. (*11*), the above approach seems both sound and practical. In these studies, we carried out the analytical calculations for the A- and B-type adsorption systems with $\varepsilon = 10^{-20}$. It should be stressed that, when in our exploratory studies ε had been set at an even lower value, the obtained results were virtually identical.

In Table III, the analytical-calculation parameters as well as the corresponding simulation parameters are summarized. The only notable difference between the simulation parameters for the A- (Table III) and AB-type adsorption systems (Table I) is that, for the latter, $K'_B = 0$.

In Fig. 4 are presented the dimensionless chronopotentiometric and dimensionless CRDCP curves (the first cycle, i.e., the first cathodic and anodic current steps) for the A-type adsorption systems obtained from the simulations (○) and analytical equations (solid lines). Figures 4a-1 and 4a-2 compare dimensionless chronopotentiometric curves (Fig. 4a-1 for $\mu = 0$ and Fig. 4a-2 for $\mu = 0.5$) obtained from the simulations (○) and analytical equations (solid lines) (*38*), (*39a*), and (*39b*). Figures 4b-1 and 4b-2 compare dimensionless CRDCP curves (Fig. 4b-1 for $\mu = 0$ and Fig. 4b-2 for $\mu = 0.5$).

In Table IV, the dimensionless chronopotentiometric and CRDC curve parameters for the A-type adsorption systems ($\mu = 0$ and $\mu = 0.5$) obtained from both the simulations and analytical equations are summarized.

TABLE III
Analytical-calculation parameters and corresponding simulation parameters for A-type adsorption systems

$Z_A = Z_B = 3s^{-1/2}$ $D_A = D_B$ $\frac{\sqrt{D_A}}{K_A}$, $s^{-1/2}$	$\Omega = \mu = 0$ and $\mu = 0.5$ $d = 1$ $K'_B = 0$ Simulation parameters		
	$\sqrt{\tau_1^{ads}}$ Eq. (*22*)	K'_A Eq. (*27*)	$\bar{I}$ Eq. (*23*)
Diff	0.333333	0.000000	0.886227
1	0.779855	1.282290	2.073385
0.1	2.088585	4.787930	5.552882
0.05	2.889617	6.921333	7.682568
0.01	6.276829	15.931612	16.68808

TABLE IV
Comparison of parameters of dimensionless chronopotentiometric and CRDCP curves for A-type adsorption systems obtained from digital simulations and analytical equations (in parentheses) for the first cycle

$\frac{\sqrt{D_A}}{K_A}$, $s^{-1/2}$	$\Omega = \mu = 0$				$\mu = 0.5$			
	$\bar{\tau}_1$	$\bar{\tau}_2$	$R_y^{1,2}$	$\Delta p^{2,1}$	$\bar{\tau}_1$	$\bar{\tau}_2$	$R_y^{1,2}$	$\Delta p^{2,1}$
Diff	1.0001 (1.0000)	0.3334 (0.3333)	3.0007 (2.9976)	1.5423 (1.5316)	1.0001 (1.0000)	0.8729 (0.8728)	1.3516 (1.3513)	1.9473 (1.9406)
1.00	1.0000 (1.0000)	0.3334 (0.3333)	4.0728 (4.0732)	0.4273 (0.4271)	1.0000 (1.0000)	0.5245 (0.5245)	2.8540 (2.8542)	0.7829 (0.7808)
0.10	1.0000 (1.0000)	0.3334 (0.3333)	4.4349 (4.4352)	–0.0150 (–0.0148)	1.0000 (1.0000)	0.3984 (0.3984)	3.8888 (3.8884)	0.1423 (0.1434)
0.05	1.0000 (1.0000)	0.3334 (0.3333)	4.4922 (4.4918)	–0.08553 (–0.08556)	1.0000 (1.0000)	0.3797 (0.3796)	4.0839 (4.0844)	0.0309 (0.0314)
0.01	1.0000 (1.0000)	0.3334 (0.3333)	4.5710 (4.5706)	–0.1853 (–0.1855)	1.0000 (1.0000)	0.3542 (0.3542)	4.3747 (4.3749)	–0.1298 (–0.1305)

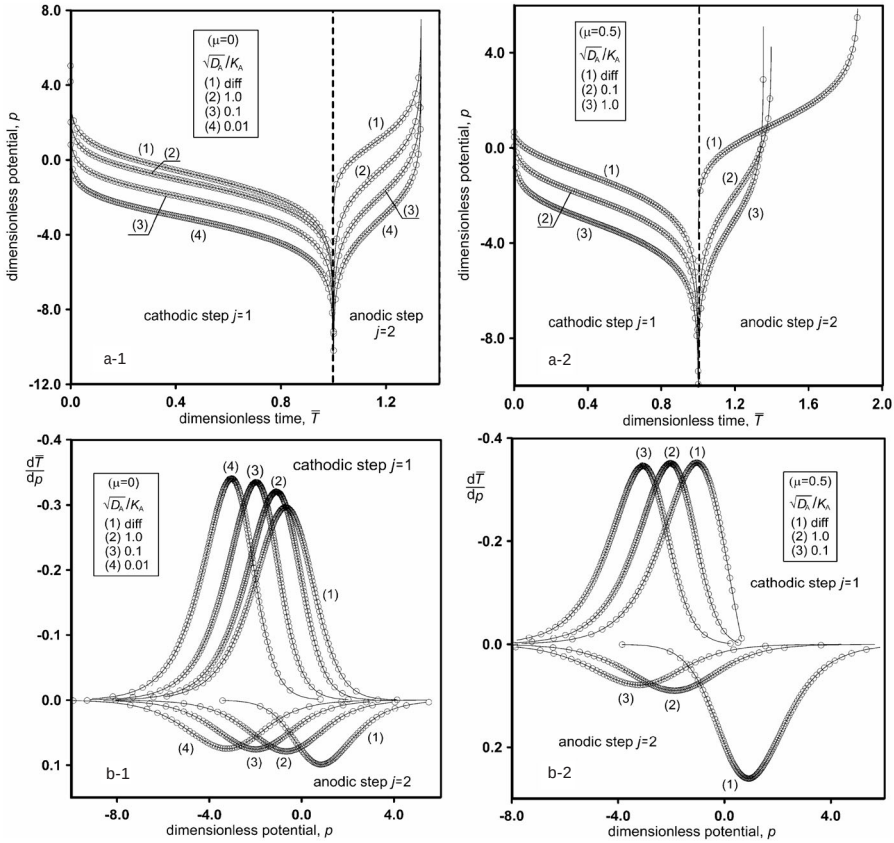

FIG. 4

First cycle of cyclic chronopotentiometry and CRDCP. Comparison of potential–time response curves (Fig. 4a-1 for μ = 0, Fig. 4a-2 for μ = 0.5) and $d\overline{T}/dp$ vs dimensionless potential, p, curves (Fig. 4b-1 for μ = 0, Fig. 4b-2 for μ = 0.5) for A-type adsorption systems obtained from analytical equations (solid lines) and simulations (○). $\sqrt{D_A}/K_A$ in $s^{-1/2}$ are: (1) diff, (2) 1.0, (3) 0.1, (4) 0.01. For clarity, only selected curves and reduced number of simulation points are presented

The B-Type Adsorption Systems ($K'_A = 0$, $K'_B \neq 0$)

For the B-type adsorption systems, the simulations were carried out only for systems for which μ = 0 or μ = 0.1. Unlike for the AB- and A-type adsorption systems, for which μ = 0.5, for the B-type adsorption systems this parameter was set at a different value. This stems from the fact that for such systems the anodic dimensionless transition time, $\overline{\tau}_2$, is extremely large in compari-

son with the dimensionless cathodic transition time, $\bar{\tau}_1$. This is especially true for large values of both K'_B and μ that lead to impractically time-consuming simulations (see also Table 5 in Molina et al.[3]). Because for the systems of this type the initial concentration of species B is greater than zero ($\mu \neq 0$), both the measurements and simulations can be started from the anodic step. Therefore, the B-type adsorption systems can be treated analogously to their A-type counterparts (with $\mu' = \mu^{-1}$).

In Table V, the analytical-calculation parameters and the corresponding simulation parameters are summarized.

In Fig. 5 are presented the dimensionless chronopotentiometric and dimensionless CRDCP curves (the first cycle, i.e., the first cathodic and anodic current steps) for the B-type adsorption systems obtained from the simulations (○) and analytical equations (solid lines). Figures 5a-1 and 5a-2 compare dimensionless chronopotentiometric curves (Fig. 5a-1 for $\mu = 0$ and Fig. 5a-2 for $\mu = 0.1$) obtained from the simulations (○) and analytical equations (solid lines) (*38*), (*39a*), and (*39b*). Figures 5b-1 and 5b-2 compare dimensionless CRDCP curves (Fig. 5b-1 for $\mu = 0$ and Fig. 5b-2 for $\mu = 0.1$).

TABLE V
Analytical-calculation parameters and corresponding simulation parameters for B-type adsorption systems

$Z_A = Z_B = 3s^{-1/2}$ $D_A = D_B$ $\frac{\sqrt{D_B}}{K_B}$, $s^{-1/2}$	$\Omega = \mu = 0$ and $\mu = 0.1$ $d = 1$ $K'_A = 0$ Simulation parameters		
	$\sqrt{\tau_1^{ads}}$ Eq. (*22*)	K'_B Eq. (*28*)	$\bar{I}$ Eq. (*23*)
Diff	0.333333	0.000000	0.886227
1	0.333333	3.000000	0.886227
0.1	0.333333	30.00000	0.886227
0.05	0.333333	60.00000	0.886227
0.01	0.333333	300.0000	0.886227

In Table VI, the parameters for the dimensionless chronopotentiometric and CRDCP curves for the B-type adsorption systems (for $\mu = 0$ and $\mu = 0.1$) obtained from both the analytical equations (*38*), (*39a*), and (*39b*), and simulations are compared.

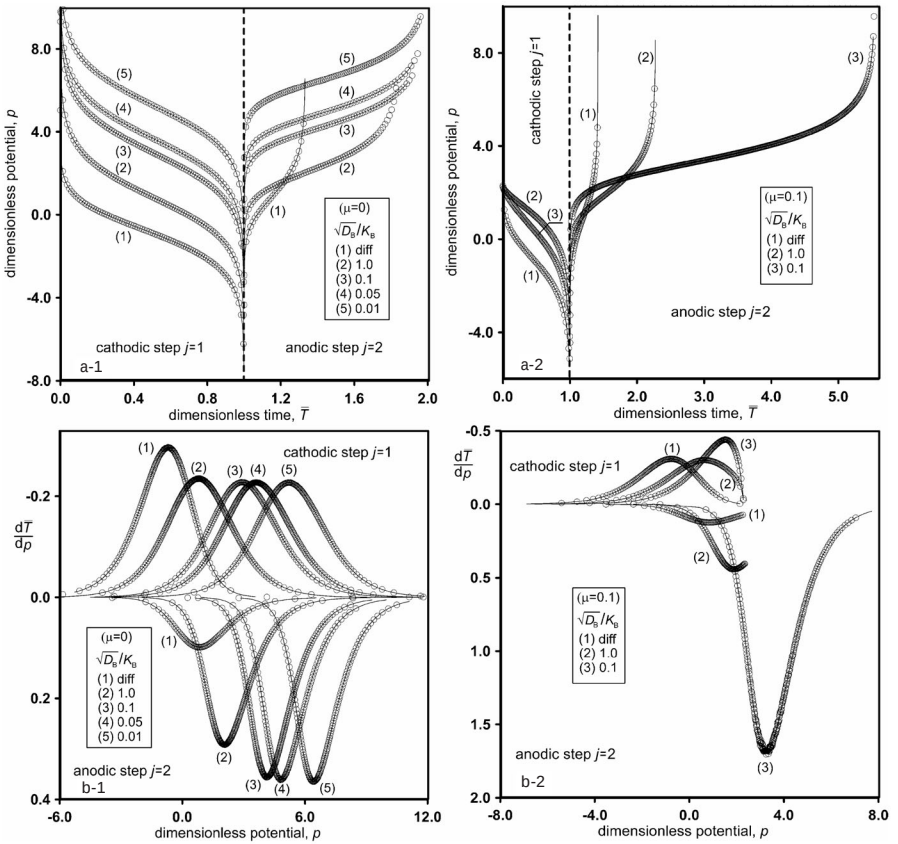

FIG. 5

First cycle of cyclic chronopotentiometry and CRDCP. Comparison between potential–time response curves (Fig. 5a-1 for $\mu = 0$, Fig. 5a-2 for $\mu = 0.1$) and $d\overline{T}/dp$ vs dimensionless potential, p, curves (Fig. 5b-1 for $\mu = 0$, Fig. 5b-2 for $\mu = 0.1$) for B-type adsorption systems obtained from analytical equations (solid lines) and simulations (○). $\sqrt{D_B} / K_B$ in $s^{-1/2}$ are: (1) diff, (2) 1.0, (3) 0.1, (4) 0.05, (5) 0.01. For clarity, only selected curves and reduced number of simulation points are presented

TABLE VI
Comparison of parameters of dimensionless chronopotentiometric and CRDCP curves for B-type adsorption systems obtained from digital simulations and analytical equations (in parentheses) for the first cycle

$\frac{\sqrt{D_B}}{K_B}$, $s^{-1/2}$	Ω = μ = 0				μ = 0.1			
	$\bar{\tau}_1$	$\bar{\tau}_2$	$R_y^{1,2}$	$\Delta p^{2,1}$	$\bar{\tau}_1$	$\bar{\tau}_2$	$R_y^{1,2}$	$\Delta p^{2,1}$
Diff	1.0001 (1.0000)	0.3334 (0.3333)	3.0007 (2.9976)	1.5423 (1.5316)	1.0001 (1.0000)	0.4161 (0.4161)	2.5191 (2.5189)	1.5973 (1.5969)
1.00	1.0001 (1.0000)	0.8417 (0.8417)	0.8050 (0.8050)	1.2655 (1.2657)	1.0001 (1.0000)	1.2723 (1.2723)	0.6815 (0.6813)	1.1525 (1.1520)
0.10	1.0001 (1.0000)	0.9799 (0.9799)	0.6401 (0.6403)	1.2125 (1.2139)	1.0001 (1.0000)	0.45275 (0.45375)	0.2757 (0.2761)	1.8015 (1.8019)
0.05	1.0001 (1.0000)	0.9898 (0.9898)	0.6299 (0.6306)	1.2098 (1.2106)	1.0001 (1.0000)	7.9924 (7.9926)	0.1536 (0.1538)	2.1092 (2.1095)
0.01	1.0001 (1.0000)	0.9979 (0.9979)	0.6268 (0.6270)	1.2089 (1.2098)	1.0001 (1.0000)	35.3521 (35.3521)	0.0320 (0.0319)	2.6481 (2.6478)

In Fig. 6, a comparison is made between the dimensionless chronopotentiometric (Fig. 6a-1) and CRDCP (Fig. 6a-2) curves obtained from the analytical equations (*38*), (*39a*), and (*39b*), and simulations for the last, 25-th step (j = 49, the last cathodic step and j = 50, the last anodic step) for a selected AB- and B-type adsorption systems.

Finally, in Table VII, the total duration times , $\overline{T}_{total}$ (j = 50, Eq. (*21*)), for the first 25 cycles of the cyclic chronopotentiometry experiments, obtained from the simulations and analytical equations, for all types of adsorption systems are summarized. Additionally, the corresponding values for a system in which neither species A nor B undergoes adsorption (diff) are also summarized.

The data presented above demonstrate that for the adsorption systems of all types, there is an excellent match between the results derived from the simulation scheme we proposed at the onset of this research and the earlier, derived from the analytical equations, results reported by Molina et al.[3] The agreement between the two sets of results encompasses not only the chronopotentiometric-curve parameters (transition times) and CRDCP-curve parameters (the ratio of the cathodic and anodic dimensionless peak heights, $R_y^{j-1,j}$, and the distance between the cathodic and anodic dimensionless peak potentials, $\Delta p^{j,j-1}$), but it also includes the shape of the chronopotentiometric and CRDCP curves. From the data presented in

TABLE VII

Duration times of the first 25 cycles in cyclic chronopotentiometry obtained from digital simulations and analytical equations (in parentheses) for adsorption systems studied

$\frac{\sqrt{D_i}}{K_i}$, $s^{-1/2}$	Total simulation time, $\bar{T}_{total}$ (j = 50)					
	AB (i = A and B)		A (i = A)		B (i = B)	
	μ = 0	μ = 0.5	μ = 0	μ = 0.5	μ = 0	μ = 0.5
1.00	40.2611 (40.2698)	63.9268 (63.9380)	15.9504 (15.9520)	26.3822 (26.3810)	55.8377 (55.8319)	69.4728 (69.4630)
0.10	46.4544 (46.4691)	70.4274 (70.4378)	9.9843 (9.9885)	12.9095 (12.9117)	69.9098 (69.9008)	129.3487 (129.3058)
0.05	47.4329 (47.4534)	71.5189 (71.5423)	9.0732 (9.0767)	11.0023 (11.0059)	71.1004 (71.0932)	171.4727 (171.4033)
0.01	48.8019 (48.8310)	73.0999 (73.1238)	7.8800 (7.8845)	8.6427 (8.6471)	72.1083 (72.0427)	439.9677 (439.7692)
Diff	22.4700 (22.4682)	48.7290 (48.7173)				

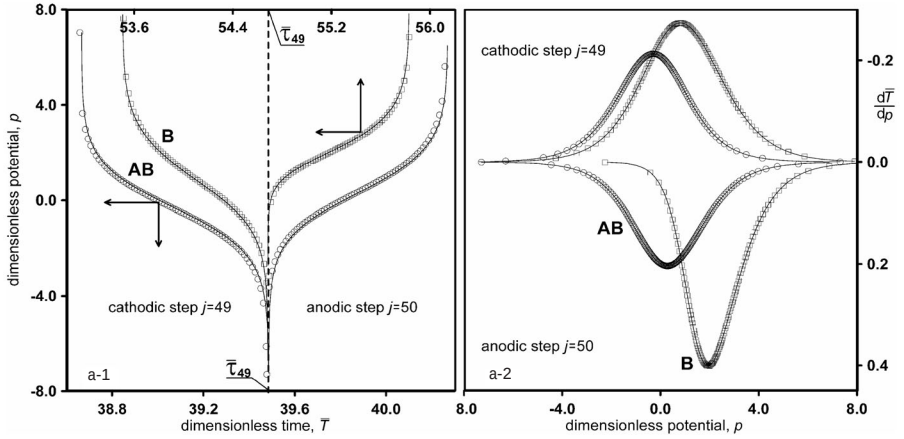

FIG. 6

Potential–time response curves (Fig. 6a-1) and CRDCP curves (Fig. 6a-2) (25-th cycle, j = 49 and j = 50) for AB-type and B-type adsorption systems ($\sqrt{D_i}$ / K_i = 1.0$s^{-1/2}$, μ = 0) obtained from analytical equations (solid lines) and simulations (○ for AB-type and □ for B-type adsorption system)

Fig. 1a-2 that compare the dependence of the relative transition times, $\bar{\tau}_{ref}$, on the current-step number, *j*, for the adsorption systems of AB-types with $\mu = 0$, it is apparent that both our simulations and Molina's analytical equations lead to exactly the same results. The same holds true for the first and second dimensionless transition times, $\bar{\tau}_1$ and $\bar{\tau}_2$, compiled in Tables II, IV, and VI. With Eq. (*43*) in mind, it can also be concluded that the dimensionless transition times, $\bar{\tau}_j$ (for all the 50 current steps studied), are also in perfect agreement. Although the values of the err function defined by Eq. (*44*) increase steadily (Fig. 1a-1) with the additional current steps taken, it can be noticed that, even at the end of the simulation, the err function reaches an acceptable value (err ≈ –3). For all the systems studied, we arrived at the first dimensionless transition time $\bar{\tau}_1 = 1.0000 \pm 1.0 \times 10^{-4}$ (it needs to be recalled here that for both the analytical equations and simulations, the time increment was set at $\delta\bar{T} = 1.0 \times 10^{-4}$). Not only does this prove that the reference time scale, $\tau = \tau_1^{ads}$, was selected properly, but it also validates the analytical equations introduced by Molina et al.[2]

The analysis of the chronopotentiometric curves presented in Figs 2a-1 and 2a-2 (for the AB-type systems), Figs 4a-1 and 4a-2 (for the A-type system), and Figs 5a-1 and 5a-2 (for the B-type system) makes it possible to conclude that our digital simulations faithfully reconstructed all the curves for the first full cycle (comprising a cathodic and anodic step), for the adsorption systems of all types. In Figs 2b-1 and 2b-2 (for the AB-type systems), Figs 4b-1 and 4b-2 (for the A-type systems), and Figs 5b-1 and 5b-2 (for the B-type systems) the CRDCP curves were compared and, as previously, the simulation and analytical results are in perfect agreement. In addition, in Tables II, IV, and VI, the CRDCP-curve parameters (i.e., the ratio of the cathodic and anodic peak heights, $R_y^{1,2}$, and the distance between the cathodic and anodic dimensionless peak potentials, $\Delta p^{2,1}$) were compared. The relative error (when the analytical values are considered to be equal to the actual values) in calculating $R_y^{1,2}$ does not exceed 0.16% in any case, whereas the absolute error in calculating $\Delta p^{2,1}$ never exceeds 0.0107 of the *p* unit. Therefore, it is apparent that, in this case, the results obtained by the two methods are very similar, indeed.

In order to demonstrate the applicability of our simulation scheme to the study and analysis of multicyclic processes, the comparison was made (Fig. 6) between the dimensionless chronopotentiometric (Fig. 6a-1) and CRDCP curves (Fig. 6a-2) obtained for the last cycle studied (25-th cycle, i.e., $j = 49$, the last cathodic step; and $j = 50$, the last anodic step). As it was the case for the first cycle (vide supra), the curves obtained here were also very similar.

In Table VII, the total duration times, $\overline{T}_{\text{total}}$, for the first 25 chronopotentiometric cycles, equal to the sum of the first 50 dimensionless transition times as defined by Eq. (*21*), were compared. Again, the agreement between the results derived from the digital simulations and analytical equations is very good, i.e., in no case the relative error exceeds 0.1%.

In summary, the research presented herein focused on the application of digital simulations to modeling cyclic chronopotentiometry and CRDCP for systems in which reactant A and/or product B undergoes adsorption at a planar electrode. Our findings are in perfect agreement with the previously reported results that have been obtained from the analytical equations describing changes in the surface concentration of the electroactive species during a multicyclic chronopotentiometric process[2,3]. Not only did we confirm the accuracy of the aforementioned analytical equations, but we also demonstrated that our simulation scheme could be successfully applied to studies of cyclic chronopotentiometry and CRDCP even in multicyclic systems. The simulation scheme we introduced can be easily adapted (after the replacement of the constant dimensionless current, $\bar{I}$, in Eq. (*26*), with appropriate current–time function) to modeling cyclic chronopotentiometry and CRDCP with programmed currents of any form without any restrictions imposed on values of the adsorption constants. In Fig. 7 are presented the dimensionless chronopotentiometric and dimensionless CRDCP curves for the AB-type adsorption system obtained from the simulations for the most popular programmed currents, i.e., for an exponential current–time function of the form

$$\bar{I}(\overline{T}) = \bar{I}_0 \exp(\omega \overline{T}_j) \tag{47}$$

and for a power current–time function of the form

$$\bar{I}(\overline{T}) = \bar{I}_0 \overline{T}_j^{\,u} \tag{48}$$

where $\bar{I}_0$ is the dimensionless initial current for an exponential current–time function and constant factor, which multiplies to $\overline{T}_j^{\,u}$ for a power–time function, ω and u are positive constants and $\overline{T}_j$ is the dimensionless time that passed since the beginning of the j-th current step.

Figures 7a-1 and 7a-2 compare dimensionless chronopotentiometric curves for several ω and u values (Fig. 7a-1 for the exponential current–time functions and Fig. 7a-2 for the power–time functions) obtained from the

simulations. Figures 7b-1 and 7b-2 compare dimensionless CRDCP curves (Fig. 7b-1 for the exponential current–time functions, and Fig. 7b-2 for the power–time functions).

Our flexible simulation scheme can be also modified and used to study processes taking place at electrodes of different than planar geometries (i.e., spherical, cylindrical, microelectrodes, etc.). It can also be applied to the study and analysis systems obeying other isotherms, such as the Langmuir

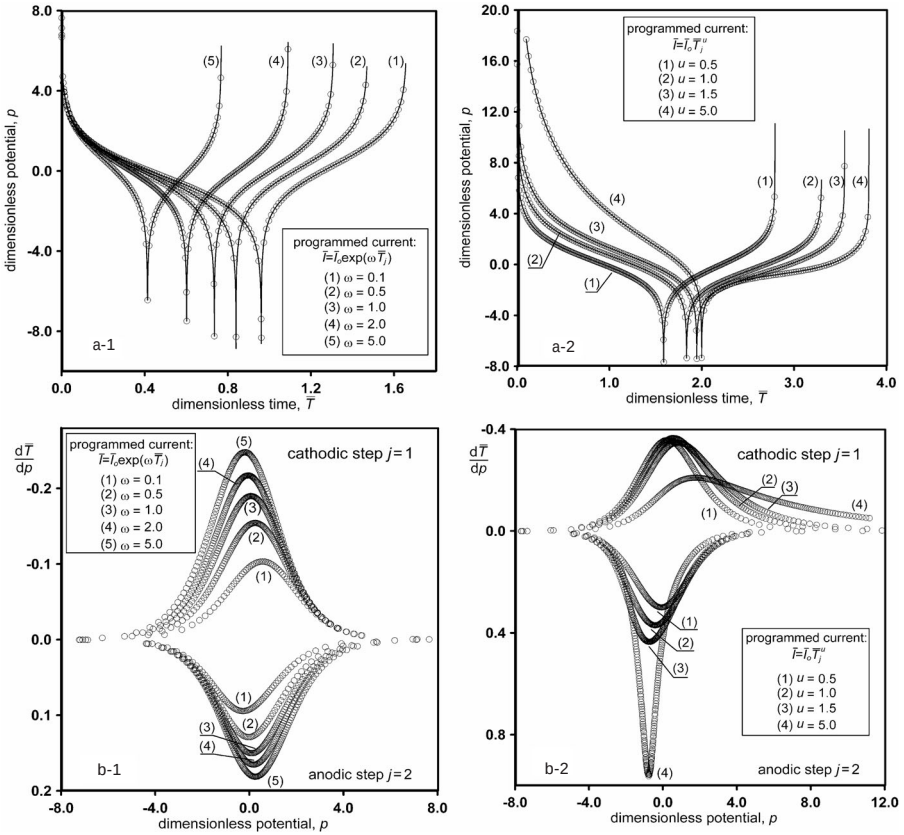

FIG. 7

Programmed current chronopotentiometry. First cycle of cyclic chronopotentiometry and CRDCP for exponential (Figs 7a-1 and 7b-1) and power–time current functions (Figs 7a-2 and 7b-2) for AB-type adsorption system ($\sqrt{D_A}$ / K_A = $\sqrt{D_B}$ / K_B = 1.0$s^{-1/2}$, $\bar{I}_0$ = $\sqrt{\pi}$/2) obtained from simulations for various ω (0.1–5.0) and *u* (0.5–5.0) parameters

or Frumkin isotherm, which describe real-life systems more accurately. Moreover, our simulation scheme can be successfully used to model cyclic chronopotentiometry for adsorption systems in which the electrode process is not fully reversible, i.e., for systems with any degree of reversibility of the charge transfer step (i.e., quasi-reversible, quasi-irreversible, and irreversible charge transfer). The studies in this area are ongoing and their results will be reported in due course.

The author thanks Dr T. S. Fekner (Ohio State University) for interesting discussions and critical remarks.

REFERENCES

1. Britz D.: *Int. J. Electrochem. Sci.* **2006**, *1*, 379; and references therein.
2. Molina A., Alcaraz M.-L., Saavedra F., Gonzáles J.: *Electrochim. Acta* **1998**, *44*, 1263.
3. Molina A., Gonzáles J., Saavedra F., Abrantes L. M.: *Electrochim. Acta* **1999**, *45*, 761.
4. Honeychurch M. J.: *J. Electroanal. Chem.* **1998**, *445*, 63.
5. Honeychurch M. J., Ridd M. J.: *Electroanalysis* **1995**, *7*, 1041.
6. Komorsky-Lovric S., Scholz F.: *J. Electroanal. Chem.* **1998**, *445*, 81.
7. Abrantes L. M., Gonzáles J., Molina A.: *Electrochim. Acta* **1999**, *45*, 457.
8. Molina A., Gonzáles J., Moreno M. M.: *Electroanalysis* **2002**, *14*, 281.
9. Gonzáles J., Molina A.: *Langmuir* **2001**, *17*, 5520.
10. Chen L., Wang Z., Lu X., Han W., Bi S.: *Electrochim. Acta* **2006**, *51*, 5548.
11. Wang J., Cai X., Wang J., Jonsson C., Palecek E.: *Anal. Chem.* **1995**, *67*, 4065.
12. Milner D. F., Weaver M. J.: *Anal. Chim. Acta* **1987**, *198*, 245.
13. Bi S., Yu J., Ye L., He B.: *Instrum. Sci. Technol.* **2000**, *28*, 303.
14. Bi S., Yu J., He B., Wang J., Qian H.: *Instrum. Sci. Technol.* **2001**, *29*, 17.
15. Bieniasz L. K., Britz D.: *Pol. J. Chem.* **2000**, *78*, 1195.
16. Britz D.: *Digital Simulation in Electrochemistry*, 3rd ed. Springer, Berlin 2005.
17. Koutecký J., Čižek J.: *Collect. Czech. Chem. Commun.* **1957**, *22*, 914.
18. Bieniasz L. K.: *Comput. Chem.* **1996**, *20*, 403.
19. Heinze J., Störzbach M., Mortensen J.: *J. Electroanal. Chem.* **1984**, *165*, 61.
20. Britz D., Heinze J., Mortensen J., Störzbach M.: *J. Electroanal. Chem.* **1988**, *240*, 27.